Available online at www.sciencedirect.com
SCIENCE DIRECT®
Journal of Solid State Chemistry 177 (2004) 2749–2755
JOURNAL OF SOLID STATE CHEMISTRY
http://elsevier.com/locate/jssc

Structural phase transition and magnetic properties of the $Sr_2FeRe_{1-x}B_x'O_6$ (B' = Nb, Ta; $x = 0$, 0.1) double perovskites

J.J. Blanco, M. Insausti, L. Lezama, J.P. Chapman, I. Gil de Muro, and T. Rojo*

Facultad de Ciencia y Tecnología, Departamento Química Inorgánica, Universidad del País Vasco, Apdo 644, ES-48080 Bilbao, Spain

Received 10 November 2003; received in revised form 29 January 2004; accepted 4 April 2004

Abstract

The double perovskites, Sr_2FeReO_6 and $Sr_2FeRe_{0.9}M_{0.1}O_6$ (M = Nb, Ta) have been obtained by soft synthesis methods which yield homogeneous particles of micrometric grain size. The materials have been studied by X-ray and neutron powder diffraction, scanning electron microscopy and magnetic measurements. Rietveld refinements show that the compounds adopt a tetragonal $I4/mmm$ structure at high temperatures and monoclinic $P2_1/n$ below the transition temperature. The magnetic structures were determined by neutron powder diffraction at 100 and 300 K for the Sr_2FeReO_6, $Sr_2FeRe_{0.9}Nb_{0.1}O_6$ and $Sr_2FeRe_{0.9}Ta_{0.1}O_6$ phases, respectively. Evidence for a ferrimagnetic coupling between the Fe^{3+} and Re^{5+} sublattices has been observed. Magnetic measurements yield magnetic moments lower than the theoretical ones being in accord with the antisite disorder of 25% in the $B-B'$ positions.

Keywords: Double oxides; Perovskite; Magnetism; Magnetoresistive; Structure; Neutron diffraction; Antisite disorder

1. Introduction

The Sr_2FeMO_6 (M= Mo, Re) compounds are members of the broad class of $A_2BB'O_6$ double perovskites which have attracted much attention in recent years because of their metallic and ferrimagnetic properties due to $Fe^{2+,3+}/Re^{6+,5+}$ and $Fe^{2+,3+}/Mo^{6+,5+}$ valence degeneracy [1–3]. They exhibit fairly large intergrain-tunneling magnetoresistance at temperatures above 400 K, which makes these double perovskites suitable candidates for technological applications in magnetoresistive devices operating at room temperature.

The physical behavior of these double perovskites is related to the fully spin polarized half-metallic (HM) electronic structure obtained in band calculations for the ferromagnetic state (FM). This state has often been called ferrimagnetic because the hybridization between d orbitals of the Fe and M atoms induces non-vanishing spin magnetic moments also at the M sites, which are aligned antiferromagnetically with respect to those of Fe [4–6].

Nevertheless, some experimental facts are not in good accord with this model. For Sr_2FeMoO_6 and Sr_2FeReO_6 the saturation magnetization is always lower than the ideal value expected for the 100% polarized HM electronic state. Using results of first-principles band structure calculations, it has been proposed that the lowering of the saturation is due to either the alternating breathing distortion of the FeO_6 and MO_6 octahedra or the antisite disorder at the Fe and M sites for different samples [7,8]. The antisite disorder would be also related to the low field magnetoresistance (LFMR) in such a way that the less disordered samples would exhibit higher LFMR ratios, although effects such as disorder distribution, connectivity or morphology increase their contribution [9].

Numerous studies have been performed for A-site solid solutions of ordered double perovskites [10]. The A_2FeReO_6 family covers the whole range from low resistivity metallic (Sr rich) to high resistivity insulating compounds (Ca rich) [11] and with ferromagnetic T_c values increasing in the Ba < Sr < Ca series [12].

*Corresponding author. Fax: +34-94-4648-500.
E-mail addresses: qiproapt@lg.ehu.es, qipinpem@lg.ehu.es (T. Rojo).

0022-4596/$ - see front matter © 2004 Elsevier Inc. All rights reserved.
doi:10.1016/j.jssc.2004.04.038

Recently, it has been found that the Pb_2FeReO_6 composition adopts a defect pyrochlore structure and exhibits a spin-glass behavior [13]. However, very few studies have been carried out with the aim of studying the influence of *B*-site substitutions [14]. In this way, introduction of new diamagnetic cations in the *B* site could induce new distributions of the Fe and Re cations in *B* and *B*′ sites, which could provoke modifications in the magnetic interactions and electronic properties.

The purpose of the present paper is to obtain information about these properties by substituting 10% of the rhenium ions by niobium and tantalum. It is worth mentioning the difficulty in controlling all the parameters to obtain homogeneous ordered samples; so, soft synthesis methods have been used in the preparation of these compounds. X-ray and neutron diffraction techniques have been utilized to characterize the degree of cationic antisite disorder, related to the magnetic properties.

2. Experimental section

2.1. Syntheses

The Sr_2FeReO_6 (SFRO), $Sr_2FeRe_{0.9}Nb_{0.1}O_6$ (SFRNO) and $Sr_2FeRe_{0.9}Ta_{0.1}O_6$ (SFRTO) oxides were synthesized from nanoscale precursors prepared by the following wet-chemical route using citric acid. Stoichiometric amounts of $Sr(CO_3)_2$, $Fe(NO_3)_3$, Nb_2O_5, Ta_2O_5 and Re metal were used as starting materials. Metals were converted to nitrates with dilute HNO_3, by previous addition of H_2O_2 to oxidize Re metal. Citric acid (1 mol of metal per 3 mol of acid) was added to the aqueous solution which was stirred for 1 h to ensure complexation. Ethylenglycol was then added (3/4 mol of ethylene per 1 mol of citric acid). The solution was dehydrated at 373 K in a sand bath into a gel which was slowly incinerated in a crucible over for one day at 723 K in air. Two thermal treatments under Ar atmosphere, heating to 1473 K at 5°/min and between 1473 and 1673 K at 2°/min, yielded samples of high purity. Metal ion contents were determined by inductively coupled plasma atomic emission spectroscopy (ICP-AES) analysis. The results are consistent with the following stoichiometries: Sr_2FeReO_6 (Found: Sr, 33.63; Fe, 10.64; Re, 35.75; Calc.: Sr, 34.14; Fe, 10.88; Re, 36.28%), $Sr_2FeRe_{0.9}Nb_{0.1}O_6$ (Found: Sr, 33.25; Fe, 10.94; Re, 32.98; Nb, 1.69; Calc.: Sr, 34.77; Fe, 11.08; Re, 33.25; Nb, 1.84%) and $Sr_2FeRe_{0.9}Ta_{0.1}O_6$ (Found: Sr, 34.25; Fe, 10.34; Re, 32.58; Ta, 3.29; Calc.: Sr, 34.17; Fe, 10.89; Re, 32.68; Ta, 3.52%). The final products are black and they give response to the presence of a magnet at room temperature. Scanning electron microscopy reveals uniform and fine grain growth. The submicrometer size is typical of soft synthetic methods.

2.2. Experimental techniques

X-ray powder diffraction (XRD) data, obtained at room temperature on a Stoe/Stadi-P diffractometer with Ge(111) monochromatized Cu$K\alpha_1$ radiation, over the interval $10° \leqslant 2\theta \leqslant 100°$ in increments of 0.02° (2θ), were Rietveld [15] fitted using the GSAS program [16].

Neutron diffraction data were recorded on the high resolution powder diffractometer D1A at the Institute Laue Langevin in Grenoble. Ge (115) monochromated neutron radiation of wavelength 1.91140(7) Å was incident on samples packed into 3 mm diameter vanadium cans. Data in the angular range $10 \leqslant 2\theta \leqslant 160°$, in steps of 0.05° were collected at 100, 300 and at 'high temperature' above the magnetic transition temperature for the Sr_2FeReO_6 (523 K), $Sr_2FeRe_{0.9}Nb_{0.1}O_6$ (450 K) and $Sr_2FeRe_{0.9}Ta_{0.1}O_6$ (500 K) phases. The data were Rietveld [15] fitted using the FullProf program [17]. A pseudo-Voigt function was used to model the peaks, with the asymmetry correction proposed by Finger [18]. In all cases, the background was fitted by linear interpolation between regions where there were no Bragg peaks. $B:B'$ cation order, where B = Fe and $B' = Re_{0.9}M_{0.1}$ (M = Nb, Ta) was primarily determined from X-ray diffraction data due to the similar neutron scattering cross sections of Fe and Re (11.62 and 11.50×10^{-24} cm^2, respectively). Also, due to the inability of laboratory X-ray diffraction to distinguish Ta and Re ($Z = 73$ and 75, respectively), resonant synchrotron data were recorded for SFRTO at the Re and Ta L_{III}-edges and 'off-edge' ($\lambda = 1.17849(1)$, 1.25713(1) and 1.30001(1) Å, respectively) on the high resolution X-ray powder diffractometer BM16 at the E.S.R.F. (Grenoble, France).

Susceptibility measurements were performed in the temperature range 1.8–300 K using a QUANTUM DESIGN MPMS-7 SQUID magnetometer and in the temperature range 300–500 K in a Faraday magnetometer at magnetic fields between 0 and 7 T. The resistance and magnetoresistance vs. temperature measurements were carried out by means of a DC four-probe system with the current parallel to the applied field.

3. Results and discussion

3.1. Structural characterization

The results of the structure refinement of the X-ray patterns measured at room temperature show a tetragonal ($\sqrt{2}a_0 \times \sqrt{2}a_0 < 2c_0$) unit cell, where a_0 is the lattice parameter for the standard cubic perovskite, gave rise to the $B:B'$ cationic order 75.5(5), 74.1(4) and 77.7(4) for the Sr_2FeReO_6, $Sr_2FeRe_{0.9}Nb_{0.1}O_6$ and $Sr_2FeRe_{0.9}Ta_{0.1}O_6$ phases, respectively. No influence of

the niobium and tantalum substitutions is observed in the partial occupation of the Fe sites by the Re ion, under these synthetic conditions. Attempts to refine the substituents (Nb, Ta) exclusively at the Fe site or a statistical mixture over the Fe and Re sites gave rise to worse residual parameters, $R_p(\%)$, $R_{wp}(\%)$, $R_{exp}(\%)$ and $R_{mag}(\%)$ and χ^2 values than the refinement at the Re site. In the case of SFRTO, resonant synchrotron data were recorded and the independent refinement of all possible substituents over the two sites gave refined fractions of $(Fe_{0.707(7)}Re_{0.301(7)}Ta_{0.020(5)})_B(Re_{0.625(5)}Fe_{0.288(7)}Ta_{0.088(8)})_{B'}$ indicating that the Ta ion substitutes, almost exclusively, at the Re site. Therefore, Ta fraction was fixed at 0.10 during subsequent refinements.

Neutron diffraction measurements showed all samples to have tetragonal $\sqrt{2}a_0 \times \sqrt{2}a_0 < 2c_0$ cells above their magnetic transition temperatures, T_c, which are around 400 K. Attempts to refine any rotation of the Jahn-Teller distorted BO_6 octahedra did not significantly improve the fit and gave parameters equal to the 'ideal' $I4/mmm$ positions within their e.s.d.'s. The refinements performed in the tetragonal unit cell show Fe atoms at 2*a* position, Re at 2*b*, Sr at 4*d*, O1 at 8 h and O2 at 4*e* crystallographic positions. At 100 and 300 K all samples showed peak broadenings, splittings and extra reflections consistent with a monoclinically distorted cell of $P12_1/n1$ symmetry. In the $P2_1/n$ space group, two crystallographically independent *B* positions (for Fe and Re) and a Sr site and three non-equivalent oxygen sites (O1, O2, O3), all in general (x, y, z) positions are described. The choice of the non-standard *b*2 setting of the $P2_1/c$ space group was chosen in order that the $a \sim b < c/\sqrt{2}$ parameters were comparable to the high temperature tetragonal symmetry. According to Glazer's notation [19], the system presents $b^-b^-c^+$ along the pseudo-cubic axes. The superscripts indicate that neighboring octahedra along the corresponding axes rotate in the same (+) or opposite (−) direction. The evolution of fits to the various temperature neutron data for SFRTO are shown in Fig. 1. Parameters refined from neutron diffraction data, and selected bond lengths and bond angles, both in space group $I4/mmm$ for all samples above their T_c and in $P12_1/n1$ below, are given in Table 1. Fig. 2 represents the evolution of the unit cell parameters for all the phases. As the monoclinic β angle varies little from 90°, it is not represented in the figure. Taking into account the structural parameters at different temperatures, the thermal variation of the unit cell parameters and volume would be related to the contraction of the unit cell due to the magnetic transition when decreasing from 500 K (paramagnetic) to 300 K (ferromagnetic).

It is worth noting that the substitution of Re by two similar and larger cations such as Nb and Ta ($r(M^{5+})$; Re = 58 pm, Ta = Nb = 64 pm) causes two different

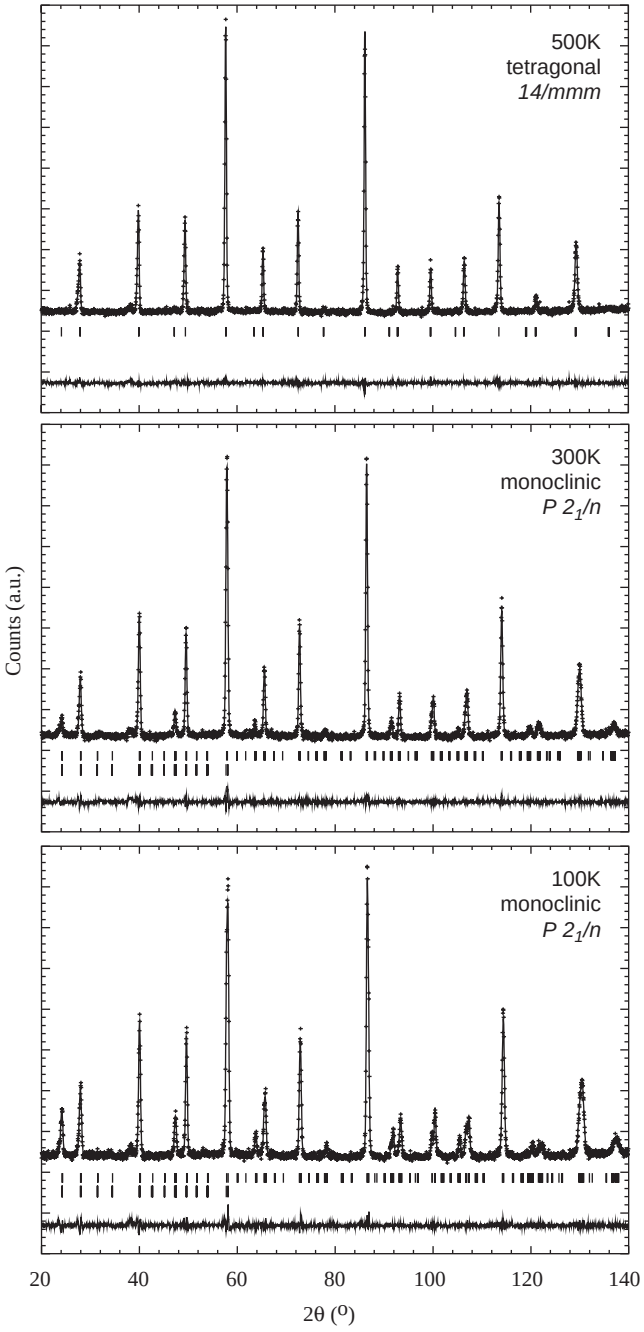

Fig. 1. Rietveld fits to the neutron powder diffraction data at 500, 300 and 100 K for the $Sr_2FeRe_{0.9}Ta_{0.1}O_6$, showing the tetragonal and monoclinic symmetries above and below T_c. For patterns at 100 and 300 K, vertical bars mark the reflections for nuclear scattering (upper) and magnetic scattering (lower).

effects in the cell. In the case of Ta, the cell is augmented but is diminished in the case of Nb. As shown in Table 1, the FeO_6 octahedra are significantly larger (expanded) than the ReO_6 octahedra. This fact is coherent with the larger ionic size of Fe^{3+} (64 pm) vs. Re^{5+} (58 pm). The average values of the $\langle$Fe–O$\rangle$ and $\langle$Re–O$\rangle$ distances are 2.009 and 1.945 Å; 1.986 and 1.958 Å; 1.999 and 1.960 Å for the Sr_2FeReO_6, $Sr_2FeRe_{0.9}Nb_{0.1}O_6$ and

$Sr_2FeRe_{0.9}Ta_{0.1}O_6$ phases, respectively. These values are in good accord with those appearing in the literature for the A_2FeReO_6 compounds (M = Ca, Sr, Ba) [20].

Table 1
Selected parameters refined from D1a neutron diffraction data for (a) Sr_2FeReO_6, (b) $Sr_2FeRe_{0.9}Ta_{0.1}O_6$ and (c) $Sr_2FeRe_{0.9}Nb_{0.1}O_6$

(a) Sr_2FeReO_6	523 K	300 K	100 K
Space group	*I*4/*mmm*	$P12_1/n1$	$P12_1/n1$
Number	*139*	*14:b2*	*14:b2*
R_p/R_{wp} (%)	7.10/9.21	7.41/9.44	7.26/9.64
Mz(*B*) (B.M.)	—	1.9(3)	2.9(2)
Mz(*B*′) (B.M.)	—	−0.6(3)	−0.9(2)
R_{mag} (%)	—	8.14	7.80
χ^2	1.26	1.41	1.36
a (Å)	5.5832(3)	5.5708(4)	5.5535(3)
b (Å)	—	5.5746(4)	5.5596(4)
c (Å)	7.9042(4)	7.9011(6)	7.8999(5)
$c/\sqrt{2}$ (Å)	5.5891(3)	5.5869(4)	5.5861(4)
β (°)	—	90.02(5)	90.03(6)
Volume (Å^3)	246.39(3)	245.37(2)	243.91(2)
'Fe'-			
O1a (Å)	1.998(5) × 4	2.019(8) × 2	1.987(6) × 2
O1b (Å)	—	2.017(7) × 2	2.014(7) × 2
O2 (Å)	2.014(8) × 2	1.992(7) × 2	2.009(6) × 2
Av B–O (Å)	*2.003(7)*	*2.009(8)*	*2.003(6)*
'Re'-			
O1a (Å)	1.949(5) × 4	1.938(8) × 2	1.951(6) × 2
O1b (Å)	—	1.931(7) × 2	1.922(7) × 2
O2 (Å)	1.938(8) × 2	1.967(7) × 2	1.947(6) × 2
Av B′–O (Å)	*1.945(6)*	*1.945(8)*	*1.940(7)*
B–O1a–*B*′ (°)	180	167.7(2)	172.3(2)
B–O1b–*B*′ (°)	180	172.8(2)	173.4(2)
B–O2–*B*′ (°)	180	172.2(2)	173.6(2)

(b) $Sr_2FeRe_{0.9}Ta_{0.1}O_6$	500 K	300 K	100 K
Space group	*I*4/*mmm*	$P12_1/n1$	$P12_1/n1$
Number	*139*	*14:b2*	*14:b2*
R_p/R_{wp} (%)	8.10/10.4	9.01/10.82	7.86/9.35
Mz(*B*) (B.M.)	—	3.2(3)	3.9(2)
Mz(*B*′) (B.M.)	—	−1.4(3)	−1.8(2)
R_{mag} (%)	—	6.10	5.56
χ^2	1.09	1.17	1.11
a (Å)	5.5963(1)	5.5733(7)	5.555(1)
b (Å)	—	5.5771(7)	5.558(1)
c (Å)	7.9232(4)	7.920(2)	7.908(1)
$c/\sqrt{2}$ (Å)	5.6026(3)	5.600(1)	5.5916(7)
β (°)	—	90.040(9)	90.05(1)
Volume (Å^3)	248.14(1)	246.17(6)	244.13(5)
'Fe'-			
O1a (Å)	2.038(6) × 4	2.011(7) × 2	1.976(7) × 2
O1b (Å)	—	2.001(6) × 2	2.008(4) × 2
O2 (Å)	1.98(2) × 2	1.98(3) × 2	1.990(5) × 2
Av B–O (Å)	*2.02(1)*	*1.999(8)*	*1.992(6)*
'Re'-			
O1a (Å)	1.919(6) × 4	1.947(7) × 2	1.970(4) × 2
O1b (Å)	—	1.952(6) × 2	1.933(5) × 2
O2 (Å)	1.98(2) × 2	1.98(1) × 2	1.97(1) × 2
Av B′–O (Å)	*1.94(1)*	*1.96(5)*	*1.959(7)*
B–O1a–*B*′ (°)	180	169.9(9)	169(1)
B–O1b–*B*′ (°)	180	171.3(8)	170.7(9)
B–O2–*B*′ (°)	180	173.8(8)	172.1(9)

Table 1 (*continued*)

(c) $Sr_2FeRe_{0.9}Nb_{0.1}O_6$	450 K	300 K	100 K
Space group	*I*4/*mmm*	$P12_1/n1$	$P12_1/n1$
Number	*139*	*14:b2*	*14:b2*
R_p/R_{wp} (%)	8.51/10.9	8.34/11.2	8.97/11.9
Mz(*B*) (B.M.)	—	2.82(25)	4.11(20)
Mz(*B*′) (B.M.)	—	−0.8(3)	−0.83(23)
R_{mag} (%)	—	9.73	5.10
χ^2	1.69	1.54	1.58
a (Å)	5.5749(3)	5.5591(3)	5.5400(4)
b (Å)	—	5.5570(3)	5.5427(4)
c (Å)	7.8892(8)	7.8839(4)	7.8777(5)
$c/\sqrt{2}$ (Å)	5.5785(5)	5.5748(3)	5.5704(4)
β (°)	—	90.15(2)	90.17(2)
Volume (Å^3)	245.20(3)	243.547(24)	241.897(29)
'Fe'-			
O1a (Å)	1.975(9) × 4	2.012(27) × 2	2.005(21) × 2
O1b (Å)	—	1.961(29) × 2	1.956(26) × 2
O2 (Å)	2.043(11) × 2	1.986(19) × 2	1.985(17) × 2
Av B–O (Å)	*1.998(10)*	*1.986(25)*	*1.982(21)*
'Re'-			
O1a (Å)	1.967(9) × 4	1.919(26) × 2	1.922(21) × 2
O1b (Å)	—	1.982(29) × 2	1.981(27) × 2
O2 (Å)	1.902(11) × 2	1.974(19) × 2	1.965(17) × 2
Av B′–O (Å)	*1.945(10)*	*1.958(25)*	*1.956(22)*
B–O1a–*B*′ (°)	180	178.0(11)	172.2(9)
B–O1b–*B*′ (°)	180	170.9(12)	169.1(10)
B–O2–*B*′ (°)	180	169.3(7)	171.2(7)

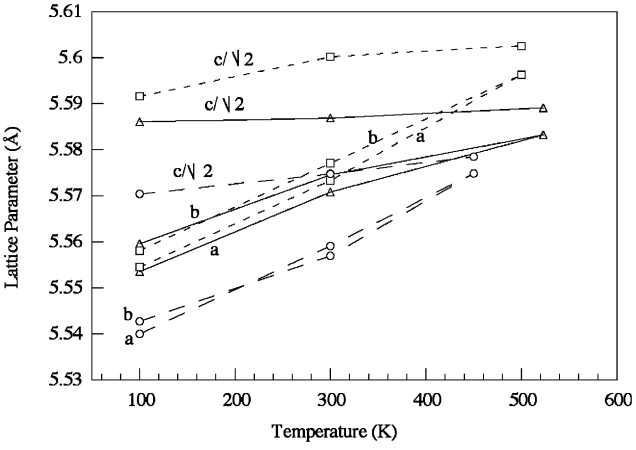

Fig. 2. Evolution of the lattice parameters *a*, *b* and $c/\sqrt{2}$ for Sr_2FeReO_6 (△), $Sr_2FeRe_{0.9}Nb_{0.1}O_6$ (○) and $Sr_2FeRe_{0.9}Ta_{0.1}O_6$ (□).

3.2. Magnetic properties

Fig. 3 shows the magnetization of the three samples registered on warming in a DC field of 0.1 kOe (0.01 kOe for the Sr_2FeReO_6 phase) after cooling in this field (FC) and without field (ZFC). The low-temperature saturation is characteristic of a spontaneous ferromagnetic (FM) ordering. Nevertheless, the values are not very significant because of the strong field dependence of

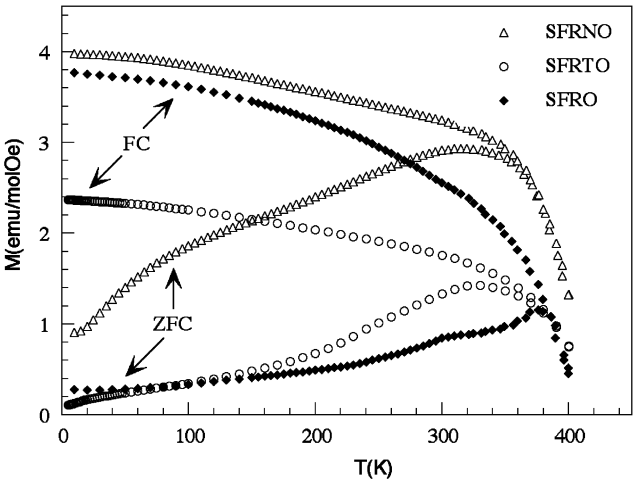

Fig. 3. Thermal evolution of the magnetization (field cooling (FC) and zero-field cooling (ZFC)) for the Sr_2FeReO_6, $Sr_2FeRe_{0.9}Nb_{0.1}O_6$ and $Sr_2FeRe_{0.9}Ta_{0.1}O_6$ phases.

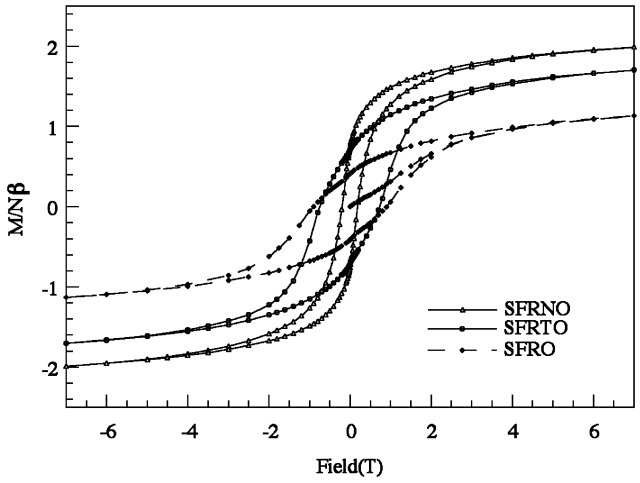

Fig. 4. Hysteresis loops at 10 K for the Sr_2FeReO_6, $Sr_2FeRe_{0.9}Nb_{0.1}O_6$ and $Sr_2FeRe_{0.9}Ta_{0.1}O_6$ phases.

the magnetization when cooling. Magnetization values at zero-field cooled (M_{ZFC}) of the phases decrease significantly below T_c. Thermomagnetic irreversibility has been currently ascribed to a spin glasslike behavior in related phases [21] but in the present case, this assignation is not so clear as long range ferromagnetic contribution has been observed by neutron diffraction. Further effects, such as magnetic anisotropy, cannot be discarded. Experimental T_c values, obtained as the minimum of the dM/dT curve by using a Faraday balance, are 400 and 420 K for the $Sr_2FeRe_{0.9}Nb_{0.1}O_6$ and $Sr_2FeRe_{0.9}Ta_{0.1}O_6$ phases, respectively. No direct relationship between these transition temperatures and the presence of a non-magnetic cation in the B' site is observed, as was previously detected in other perovskites with magnetoresistent properties [22]. As can be seen, the presence of a 10% of niobium or tantalum in a sample with around 25% of disorder in the $B-B'$ positions does not greatly affect the transition temperatures, the degree of disorder being the main factor controlling the magnetic and electronic properties in these materials.

The hysteresis loops for these samples at 5 K are shown in Fig. 4. None of them behaves as a conventional ferromagnet with a saturated magnetic moment. Although the samples show spontaneous magnetization, saturation is not achieved at 7 T. The saturation moments are lower than the theoretical value of 3.01 μ_B expected for either collinear ferromagnetic configuration $[Fe^{3+}(5\,\mu_B)][Re^{5+}(2\,\mu_B)]$ or $[Fe^{2+}(4\,\mu_B)][Re^{6+}(1\,\mu_B)]$. In this way, values of 1.1, 1.9 and 1.7 μ_B have been obtained for the SFRO, SFRNO and SFRTO phases, respectively. The lower values of the moments could be related to the antisite disorder between B and B' positions displayed in a ferromagnetic arrangement, as will be explained in the following section.

3.3. Magnetic structure

The neutron powder diffraction data at 100 K reveal a strong magnetic contribution to the low-angle reflections, especially visible at [011] Bragg position, at 23° (2θ). A ferrimagnetic structure was modeled with magnetic moments at the Fe positions parallel ordered and with Re positions in an antiferromagnetic arrangement with respect to the iron ones (Fig. 5). After the full refinement of the profile, including the magnetic moment magnitude and orientation, a discrepancy factor R_{mag} around 8% was reached. Magnetic moments were refined along each of the crystallographic axes and produced a significantly better fit to the data when refined in the z direction. Values of the refined magnetic moments, for B and B' site are shown in Table 1. The observed moments are related to the antisite disorder and could be evaluated for the simplest ferrimagnetic arrangements between B and B' sublattices which produce a net magnetization $M_S = m_B - m_{B'}$. This approximation was assumed by Balcells et al. [23] and is in accord with the Monte Carlo computation of Ogale et al. [24]. Sublattice B is occupied by $(1-x)$Fe ions and x Re ions, then $M_S = (1-x)m_{Fe} + xm_{Re} - xm_{Fe} - (1-x)m_{Re}$ where m_{Fe} and m_{Re} are the magnetic moments of Fe^{3+} and Re^{5+} ions, assuming a spin-only contribution. In this way, the calculated theoretical moments are 1.53, 1.64 and 1.86 μ_B for the SFRO, SFRNO and SFRTO phases, respectively. The small difference observed could be attributed to two factors. Firstly, it could be assumed that, locally at the antisites, superexchange pathways of Fe–O–Fe (AF), Re–O–Re and Re–O–Fe hold yielding a lower magnetic moment than predicted. Secondly, it is possible that the smaller quantities of SFRO and SFRNO compounds induced a greater imprecision in the calculation of the cation order. In this kind of

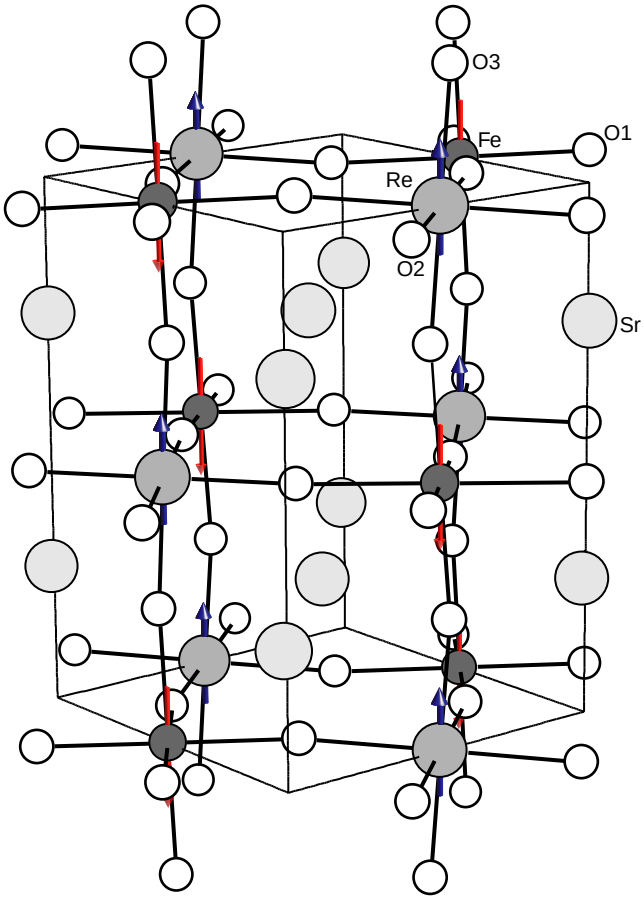

Fig. 5. Ideal structure for the Sr_2FeReO_6 phase at 100 K without mis-site disorder and magnetic moments refined in the z direction.

samples, the properties are always strongly dependent on the preparation of the sample, which clearly influences the cation disorder.

4. Conclusion

The sol–gel method has been used to synthesize the Sr_2FeReO_6, $Sr_2FeRe_{0.9}Nb_{0.1}O_6$ and $Sr_2FeRe_{0.9}Ta_{0.1}O_6$ homogeneous oxides with a grain size of around 0.3 μm. The structural refinement of X-ray diffraction data is in accord with a cationic order of 75.5(5), 74.1(4) and 77.7(4) for the SFRO, SFRNO and SFRTO, respectively. In the case of SFRTO these results have been confirmed by synchrotron X-ray data, which indicate that the Ta substitutes exclusively at the Re site. A structural phase transition from a tetragonal $I4/mmm$ cell, at T_c temperatures, to a monoclinic $P2_1/n$ symmetry has been observed by neutron diffraction measurements. At low temperatures, the magnetic structure was modeled with ferromagnetic magnetic moments at the Fe positions and with Re positions in an antiferromagnetic arrangement with respect to the iron ones. Magnetic measurements of the samples are characteristic of a spontaneous ferromagnetic ordering, although the saturation moments are lower than theoretical values. This value is related to the super-exchange pathways between the Re and Fe cations in the sublattice which results from the antisite disorder. In this way, it can be concluded that the synthesis method considerably influences the degree of disorder in the samples, this fact being responsible of the observed magnetic and electrical properties.

Acknowledgments

This work has been carried out with the financial support of the Ministerio de Educación y Ciencia (MCYT, MAT2001-0064) and University of the Basque Country (UPV, 9/UPV 00169.310-14199/2001) which we gratefully acknowledge. J.P. Chapman also thanks the Spanish Government for a PostDoctoral Fellowship. The authors would also like to thank Dr. Teresa Fernández of the ILL and Dr. Andy Fitch of the ESRF for their help in collecting diffraction data and the ILL and ESRF for the provision of beamtime.

References

[1] K.-I. Kobayashi, T. Kimura, H. Sawada, K. Terakura, Y. Tokura, Nature 395 (1998) 677.
[2] K.-I. Kobayashi, T. Kimura, Y. Tomioka, H. Sawada, K. Terakura, Y. Tokura, Phys. Rev. B. 59 (17) (1999) 11159.
[3] W. Prellier, V. Smolyaninova, A. Biswas, C. Galley, R.L. Greene, K. Ramesha, J. Gopalakrishnan, J. Phys. C. 12 (2000) 965.
[4] D.D. Sarma, P. Mahadevan, T. Saha-Dasgupta, S. Ray, A. Kumar, Phys. Rev. Lett. 85 (2000) 2549.
[5] Z. Fang, K. Terakura, J. Kanamori, Phys. Rev. B 63 (2001) 180407.
[6] J. Kanamori, K. Terakura, J. Phys. Soc. Japan 70 (2001) 1433.
[7] I.V. Solovyev, Phys. Rev. B 65 (2002) 144446.
[8] A. Ogale, S. Ogale, R. Ramesh, T. Venkatesan, Appl. Phys. Lett. 75 (1999) 537.
[9] D.D. Sarma, E.V. Sampathkumaran, S. Ray, R. Nagarajan, S. Majumdar, A. Kumar, G. Galini, T.N. Guru Row, Solid State Commun. 114 (2000) 465;
M. García-Hernández, J.L. Martínez, M.J. Martínez-Lope, M.T. Casais, J.A. Alonso, Phys. Rev. Lett. 86 (11) (2001) 2443.
[10] G. Popov, M. Greenblatt, M. Croft, Phys. Rev. B 67 (2003) 24406;
T. Alamelu, U.V. Vadaradaju, M. Venkatesan, A.P. Douvalis, J.M.D. Coey, J. Appl. Phys. 91 (10) (2002) 8909.
[11] H. Kato, T. Okuda, Y. Okimoto, Y. Tomioka, K. Oikawa, T. Kamiyama, Y. Tokura, Phys. Rev. B. 65 (2002) 144404;
T. Alamelu, U.V. Varadaraju, M. Venkatesan, A.P. Douvalis, J.M.D. Coey, J. Appl. Phys. 91 (10) (2002) 8909.
[12] S.E. Lofland, T. Scabarozi, S. Kale, S.M. Bhagat, S.B. Ogale, T. Venkatesan, R.L. Greene, J. Gopalakishnan, K. Ramesha, IEEE Trans. Magn. 37 (2001) 2153.
[13] K. Ramesha, L. Sebastian, B. Eichhorn, J. Gopalakishnan, J. Mater. Chem. 13 (2003) 2011.

[14] J.J. Blanco, T. Hernández, L.M. Rodriguez-Martínez, M. Insausti, J.M. Barandiaran, J.M. Greneche, T. Rojo, J. Mater. Chem. 11 (2001) 253.
[15] H.M. Rietveld, J. Appl. Crystallogr. 2 (1969) 65.
[16] A.C. Larson, R.B. von Dreele, GSAS: General Structural Analysis System; LANCE, MH-H805, Los Alamos National Laboratory: Los Alamos, NM 87545, USA, 1994.
[17] J. Rodriguez-Carvajal, Physica B 192 (1993) 55.
[18] L.W. Finger, D.E. Cox, A.P. Jephcoat, J. Appl. Crystallogr. 27 (1994) 892.
[19] A.M. Glazer, Acta Crystallogr. B 28 (1972) 3384;
A.M. Glazer, H. Megaw, Philos. Mag. 25 (1972) 1119.
[20] J. Gopalakrishnan, A. Chattopadhyay, S.B. Ogale, T. Venkatesan, R.L. Greene, A.J. Millis, K. Ramesha, B. Hannoyer, G. Marest, Phys. Rev. B 62 (14) (2000) 9538.
[21] M. Itoh, I. Natori, S. Kubota, K. Motya, J. Phys. Soc. Japan 63 (1994) 1486.
[22] J.J. Blanco, L. Lezama, M. Insausti, J. Gutierrez, J.M. Barandiarán, T. Rojo, Chem. Mater. 11 (12) (1999) 3464.
[23] Ll. Balcells, J. Navarro, M. Bibes, A. Roig, B. Martínez, J. Fontcuberta, Appl. Phys. Lett. 78 (6) (2001) 781.
[24] A. Ogale, S. Ogale, R. Ramesh, T. Venkatesan, Appl. Phys. Lett. 75 (1999) 537.